environments

MDPI

Article

SWAT Machine Learning-Integrated Modeling for Ranking Watershed Vulnerability to Climate Variability and Land-Use Change in Alabama, USA, in 1990–2023

Riad Arefin [1], Jonathan Frame [1], Geoffrey R. Tick [1,2], Derek D. Bussan [3], Andrew M. Goodliffe [1] and Yong Zhang [1,*]

[1] Department of Geological Sciences, University of Alabama, Tuscaloosa, AL 35487, USA; marefin1@crimson.ua.edu (R.A.); jmframe@ua.edu (J.F.); gtick@ua.edu (G.R.T.); amg@ua.edu (A.M.G.)
[2] Santa Clara Valley Water District, Groundwater Management Unit, San Jose, CA 95118, USA
[3] Derek Bussan's Consulting LLC, Durango, IA 52039, USA; bussan@okstate.edu
* Correspondence: yzhang264@ua.edu

Abstract

Understanding streamflow dynamics in watersheds affected by human activity and climate variability is important for sustainable water and environmental resource management. This study evaluates the vulnerability of Alabama watersheds to anthropogenic and climatic changes using an integrated framework combining GIS, remote sensing, hydrological modeling, and machine learning (ML). Three Soil and Water Assessment Tool (SWAT) models, differing in spatial resolution and soil inputs, were developed to simulate streamflow under baseline and land-use/land cover (LULC) scenarios from 1990 to 2023. The model, built with consistent 100 × 100 m rasters and fine-resolution SSURGO (Soil Survey Geographic Database) soil data, achieved the best calibration and was selected for detailed analysis. Streamflow trends were assessed over two periods (1993–2009 and 2010–2023) to help isolate climate variability (from LULC effects), while LULC changes were evaluated using 1992, 2011, and 2021 maps. A Long Short-Term Memory (LSTM) model further enhanced simulation accuracy by integrating partially calibrated SWAT outputs. Watershed vulnerability was ranked using a multi-criteria framework. Two watersheds were classified as highly vulnerable, nine as moderately vulnerable, and three as having low vulnerability. Basin-level contrasts revealed moderate climate impacts in the Tombigbee Basin, greater climate sensitivity in the Black Warrior Basin, and LULC-dominated impacts in the Alabama Basin. Overall, LULC change exerted stronger and more spatially variable effects on streamflow than climate variability. This study introduces a transferable SWAT–ML vulnerability ranking framework to guide watershed and environmental management in data-scarce, human-modified regions.

Keywords: arc SWAT model; climate variability; land use; watershed; machine learning; vulnerability rank

Academic Editor: Guobin Fu

Received: 1 September 2025
Revised: 17 October 2025
Accepted: 17 October 2025
Published: 21 October 2025

Citation: Arefin, R.; Frame, J.; Tick, G.R.; Bussan, D.D.; Goodliffe, A.M.; Zhang, Y. SWAT Machine Learning-Integrated Modeling for Ranking Watershed Vulnerability to Climate Variability and Land- Use Change in Alabama, USA, in 1990–2023. *Environments* **2025**, *12*, 395. https://doi.org/10.3390/environments12100395

1. Introduction

Human activities and climate variability are increasingly altering both the quantity and quality of surface water resources, with direct implications for ecosystem health and environmental sustainability. Agricultural practices, such as fertilizer and pesticide use, contribute to elevated nutrient and contaminant levels that are closely tied to streamflow dynamics [1–3]. These pollutants are mobilized through watersheds [4,5], where they interact

with soils, groundwater, and aquatic ecosystems, affecting biodiversity and water quality. In controlled watersheds, the presence of reservoirs and dams further disrupts natural hydrological regimes, altering sediment transport and nutrient cycling. Although mitigation measures such as filter strips [6], drainage modifications [7], and reduced nitrogen application [8] have been proposed, evaluating their long-term environmental effectiveness requires quantitative modeling of streamflow and pollutant transport under both natural and anthropogenic influences that fluctuate over multi-decadal timescales. Such evaluations are important for developing evidence-based strategies to support sustainable watershed management and inform environmental policy in response to climate variability and land-use change.

Hydrological models are widely used to evaluate streamflow [9,10], yet many watersheds remain ungauged or lack sufficient monitoring data. To address these data gaps, parameter estimation methods ranging from regression-based approaches [11–15] to geostatistical techniques [13,16] and similarity-based regionalization [17,18] have been developed. Among existing tools, the Soil and Water Assessment Tool (SWAT) is one of the most widely applied for assessing the impacts of land-use/land cover (LULC) change [19] and climate variability on watershed hydrology across single [9] or multiple watersheds [20]. Its strengths lie in simulating large-scale, long-term hydrological processes and in coupling with SWAT-CUP for calibration, validation, and uncertainty analysis [21–24].

Previous hydrological studies in Alabama, USA, have largely concentrated on uncontrolled watersheds [25,26]. However, the Tombigbee–Black Warrior–Alabama River Basin contains more than 30 reservoirs, creating hydrological systems shaped by both natural variability and human regulation. This highlights the need to evaluate streamflow dynamics in both controlled and uncontrolled basins. At the same time, ongoing LULC changes—particularly urban expansion and forest loss—are altering the hydrological balance by increasing surface runoff and reducing groundwater recharge [27–29]. Climatic variability further compounds these pressures through shifts in rainfall patterns and streamflow volumes [30]. Together, these interacting stressors introduce significant uncertainty in water availability, water quality, and overall watershed resilience across Alabama.

While traditional hydrological models provide valuable process-based insights, they often struggle to capture nonlinear interactions among climate variability, human interventions, and watershed response. Recent advances in machine learning (ML), especially Long Short-Term Memory (LSTM) networks, offer complementary strengths by capturing temporal dependencies in hydrological time series and improving predictions in data-scarce settings [31–36]. However, integration of ML with process-based models remains limited, particularly in regions where both controlled and uncontrolled watersheds must be considered simultaneously.

This study addresses these gaps through four objectives:

(i) Develop and calibrate SWAT models for both gauged and ungauged watersheds, extending modeling capacity to data-limited regions;
(ii) Quantify the relative contributions of LULC change and climate variability to streamflow across temporal scales;
(iii) Integrate LSTM models with process-based simulations to improve predictive accuracy, particularly for peak-flow conditions;
(iv) Establish a multi-criteria vulnerability ranking framework that incorporates physical, static, and dynamic watershed attributes in a systematic, comparable manner.

By analyzing both baseline and LULC change scenarios over more than three decades, this study provides one of the first comprehensive, basin-scale evaluations of watershed vulnerability in Alabama that accounts simultaneously for climate variability, land-use transitions, and reservoir regulation. The integrated SWAT–LSTM framework represents

a novel scientific contribution, combining process-based and data-driven approaches to improve model robustness in both gauged and ungauged watersheds. The multi-criteria ranking system delivers a transferable decision-support tool for prioritizing watershed and environmental management under competing pressures from agriculture, urbanization, and ecological demands. More broadly, the methodology advances sustainable water and environmental resource management in regions worldwide where monitoring networks are sparse and human–climate interactions are intensifying, with direct implications for water security, ecosystem services, and environmental policy.

2. Study Area

The study area encompasses the Tombigbee-Black Warrior-Alabama River Basin, covering approximately 1119 thousand square kilometers in Alabama, located in southeast United States (U.S). Agricultural activity and LULC dynamics are prominent. Prior hydrology-related measurements, e.g., water mixing, sediment supply and agroecosystem, have been conducted in and around this place [37–41], indicating elevated vulnerability to hydrologic effects. According to Grabowska [42], streamflow strongly influences the transport of dissolved constituents. In addition, given the presence of large reservoirs and an extensive stream network, SWAT is well suited to identify groundwater-sensitive parameters. According to ADECA and OWR [43], about 6% (496 million gallons per day, MGD) of Alabama's total water use is supplied from groundwater.

Figure 1a locates the study area and maps two hydrologic datasets: streamflow-monitoring (gauged) sites (both regulated and unregulated) and 35 weather stations. These points are important for reducing flood risk at cross-dam sites and within ungagged sub-basins. In total, 35 sub-basins were delineated (in Figure 1a), 32 of which contain cross-dams (Figure 1b). Among these, 9 watersheds were calibrated using available USGS streamflow monitoring data, while 7 sub-basins remain uncontrolled, 5 of which were calibrated. The region exhibits diverse lithological formations associated with the Appalachian Mountain range, largely exposed through intense weathering and erosion (Figure 2a). Reservoir properties are summarized in Tables S1 and S2: the largest reservoir by volume is W5 (Lewis Smith Reservoir) with a capacity of 2.06 billion cubic meters, while the largest by surface area is W23 (Lake Martin Reservoir), covering 16.9 thousand square kilometers. Hypsometric integral (HI) values—used to assess watershed erosional maturity—indicate that most watersheds fall within youthful to mature stages of geomorphic development (Figure 2b). The same figure also presents drainage density (DD) values for each watershed.

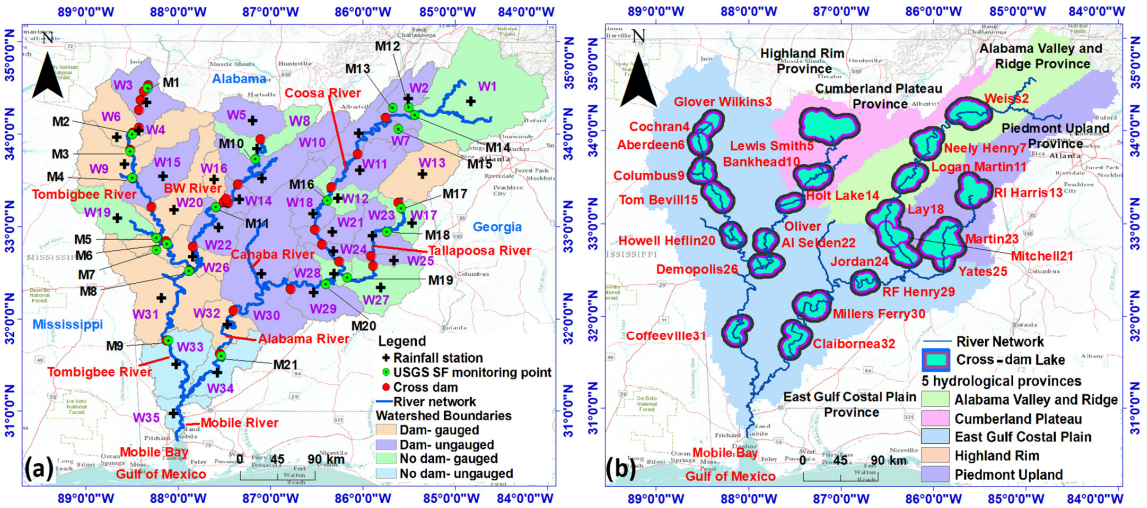

Figure 1. (**a**) Location map of the study area, showing 35 delineated watersheds (W1~W35); (**b**) Reservoir locations and the spatial distribution of hydrological provinces.

Areas with low DD but high HI (convex shape) are typically dominated by subsurface (groundwater) flow due to greater storage and slower drainage; at higher DD, this relationship reverses [44]. Figure 2c shows how the extent of five major LULC classes change over time.

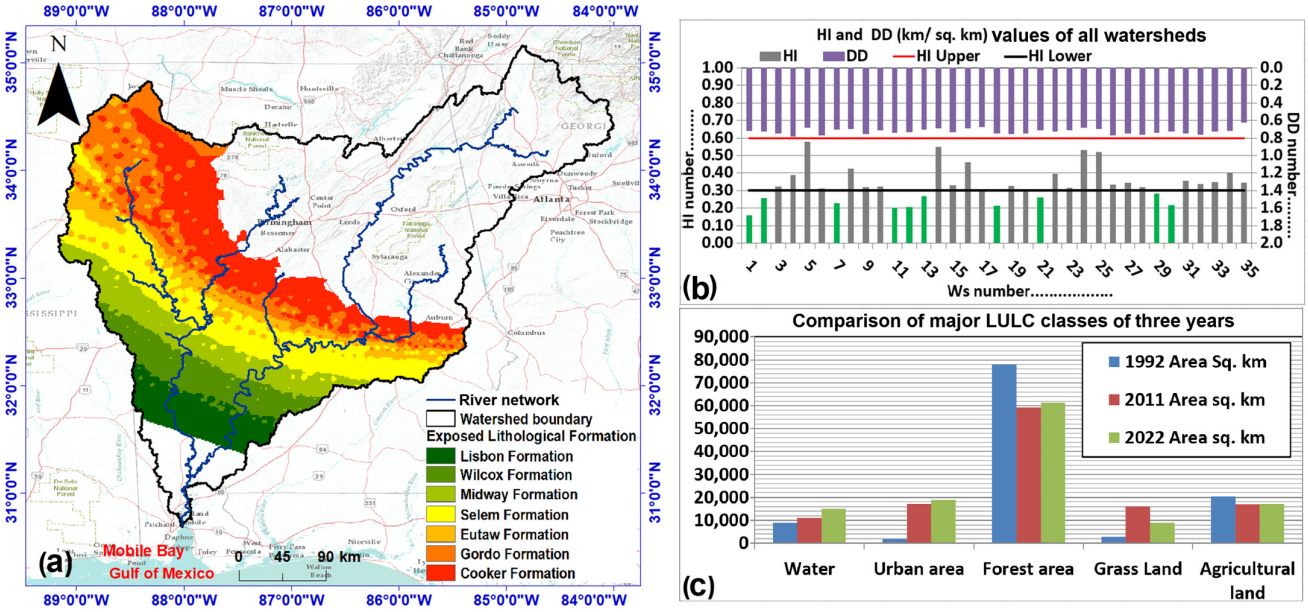

Figure 2. (**a**) Exposed lithological formations vulnerable to pollution; (**b**) Hypsometric integral (HI) values for 35 watersheds, illustrating erosional stages, where the red horizontal line distinguishes younger from mature basins, and the black line separates mature from younger basins [45]. Drainage density (DD, km/km^2) is also shown; (**c**) Yearly LULC classifications for 1992, 2011, and 2021, derived from NLCD raster data.

2.1. Rainfall Pattern

Weather stations (marked in Figure 1a), covering the period 1990–2023, were used to capture conditions ranging from near-normal to extreme drought events. Extending the analysis period strengthens the model by incorporating a wider range of dry and wet conditions [46]. Based on the 12-month Standardized Precipitation Index (SPI-12) calculated from monthly data, three major drought events were identified: 1999–2003, 2006–2009, and 2011–2013, along with several smaller events. Basically, longer timescales (9–12 months) are used to evaluate hydrological droughts, reflecting water shortages in streamflow and artificial reservoirs [47]. A holistic overview of these indices and their limitations can be found in literature [48–51]. Figure 3a–c presents SPI-12 graphs for three representative stations (sub-basins) 3, 7, and 11. Although SPI errors tend to occur during extreme droughts or very wet conditions, such variability does not substantially affect the overall reliability of the results [46].

Innovative trend analysis has been widely used to evaluate long-term rainfall patterns and the impacts of climate variability [52–58]. In this study, rainfall trends are illustrated in Figure 3d–f, where the X-axis represents the first half of the record and the Y-axis represents the second half. Most weather stations indicate decreasing rainfall trends; however, stations in watersheds W5, W7, W8, W10, W14, W15, W16, W22, W33, and W35 show increases. The strongest positive trend was observed in watershed W8 (slope = +0.0256), while the most pronounced decline occurred in watershed W34 (slope = −0.0355).

Figure 3g compares the statistical significance of the metrics across watersheds. Trend slopes span −0.036 (W2) to 0.0256 (W 29). The 95% confidence intervals have upper bounds from 0.00179 (W20) to 0.00505 (W32) and lower bounds from −0.00179 (W22) to −0.00505 (W33). Correlations are very high ($R^2 > 0.98$). The trend indicator ranges from

−0.5662 (W2) to 0.4596 (W29). The slope standard deviation varies from 0.00091 (W33) to 0.00258 (W22).

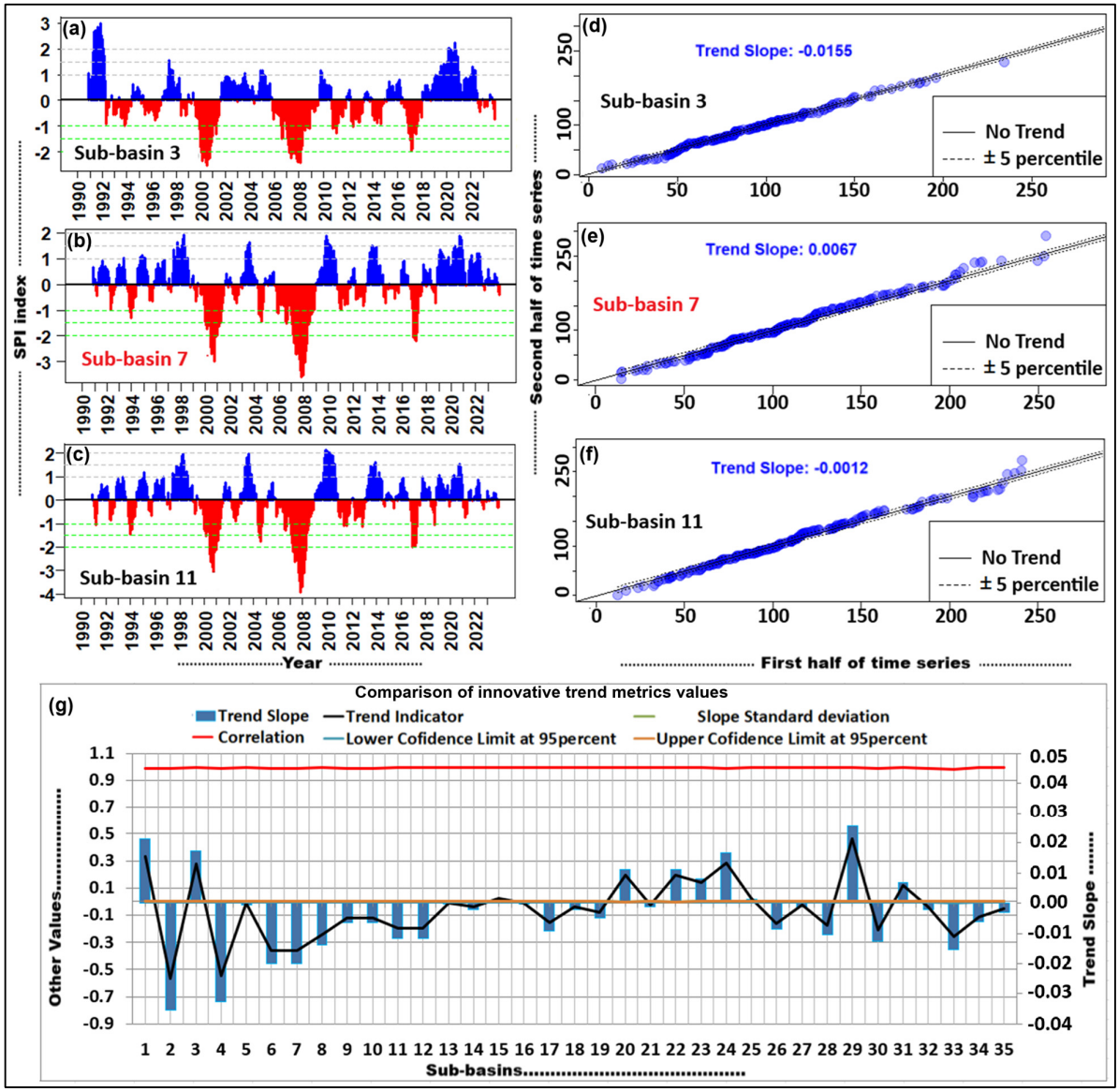

Figure 3. (**a**–**c**) Representative SPI-12 drought index graphs highlighting three major drought events (1999–2003, 2006–2009, and 2011–2013, shown in red). (**d**–**f**) Innovative trend analysis of rainfall, where the *X*-axis represents the first half of the time series and the *Y*-axis represents the second half. (**g**) All-watersheds trend graphs with different statistical parameters: the left vertical axis applies to all parameters except the trend slope, which uses the right vertical axis.

2.2. LULC Pattern

This study uses NLCD datasets from 1992 (13 LULC classes), 2011 (15 classes), and 2021 (15 classes) as model input, an approach widely applied in the U.S and consistent with prior hydrologic modeling (e.g., Kim et al. [59]). For comparative analysis, the NLCD classes were grouped into five major categories: (1) water bodies (WATR, WETF, WETN); (2) urban areas (URLD, URMD, URHD, UIDU, UCOM); (3) forests (FRSD, FRSE, FRST); (4) grasslands (RNGB, RNGE, SWRN); and (5) agricultural land (AGRR, WWHT, HAY). Abbreviations and corresponding areas are listed in Table S3, while Figure S1a–c in the Supplementary Materials illustrates comparative changes across years. Forests cover the largest proportion of land area, although total forest cover has declined over

time. Agricultural land also declined markedly, from 20,317 km^2 in 1992 to 17,196 km^2 in 2021, except for HAY, which expanded from 11,566 km^2 to 14,636 km^2. Grasslands, though decreasing in most subclasses, showed an overall increase due to expansion of RNGE and RNGB. Urban areas consistently expanded, while water bodies—particularly WETN—grew from 301 km^2 to 904 km^2 between 1992 and 2011. Similar LULC patterns have been reported across Alabama using NLCD data [26]. Google Earth Engine [60] is widely used for LULC analysis in global studies. In addition, Abburu and Golla [61] review various image classification techniques.

2.3. Soil Distribution

The earliest widely used open-source soil dataset was produced by the Food and Agriculture Organization (FAO) in 1981 [62]. In addition, a 1:5,000,000-scale World Soil Map, compiled by soil scientists over the two decades following 1961, is available. A more recent global soil database, SoilGrids (since 2016), provides higher-resolution, regularly updated soil information [63]. For this study, we used SSURGO (Soil Survey Geographic Database) developed for the United States in Models M1 and M2, and incorporated the FAO soil raster (18 soil classes) in Model M3 to characterize the study area. SSURGO soil raster supported full spatial coverage; however, STATSGO (State Soil Geographic Database) was considered as a fallback. The STATSGO database integrates geology, topography, vegetation, climate, and Landsat imagery [64]. Both SSURGO and STATSGO were developed by the U.S. Department of Agriculture's Natural Resources Conservation Service (NRCS) [65]. Their nominal mapping unit areas are ~0.02 km^2 (2 ha) for SSURGO and ~6.25 km^2 (625 ha) for STATSGO, with map scales ranging from 1:31,680 to 1:15,840 [66]. In this study, SSURGO provided the soil inputs for the hydrologic simulations, providing 5125 unique soil classes across the study area (Figure 4a,b).

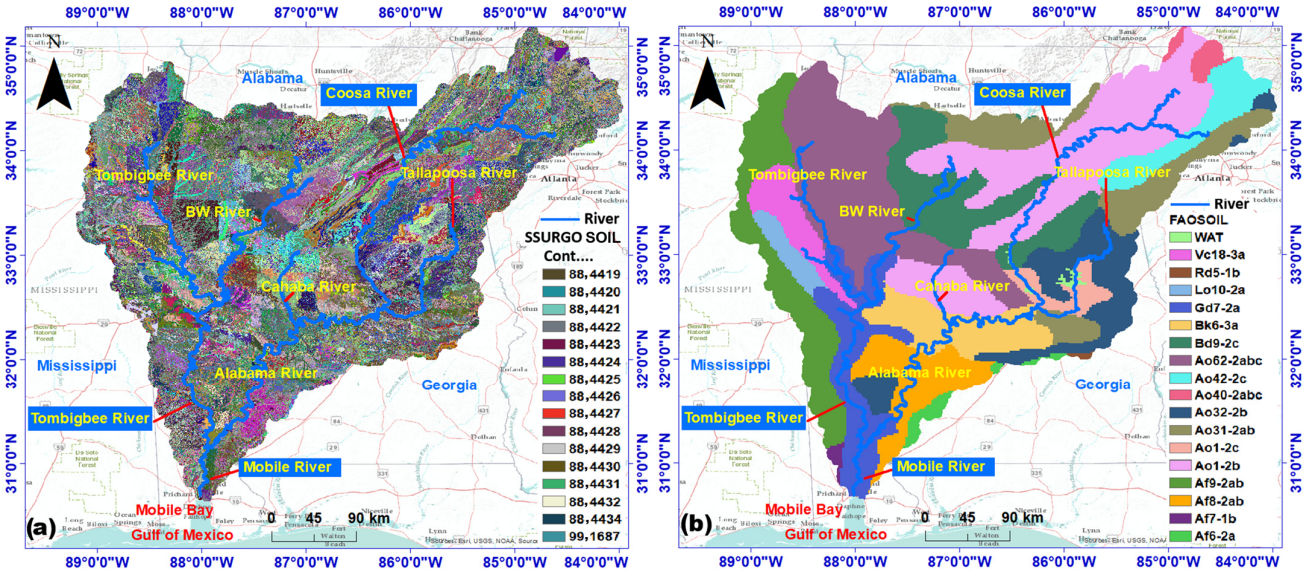

Figure 4. Soil classification maps used in the study: (**a**) Soil map from the FAO dataset; and (**b**) High-resolution soil map from the SSURGO database.

3. Sources of Data

The SWAT model requires multiple climatic inputs, including solar radiation, humidity, wind speed, precipitation, and temperature, to compute the water-balance components. In this study, these data were obtained from NASA Power (Table 1). A Digital Elevation Model (DEM) at 1-arc-second resolution, derived from the Shuttle Radar Topographic Mission (SRTM) via the USGS Earth Explorer, was used to derive watershed characteristics

such as depression fill, flow direction, flow accumulation, and watershed delineation. All rasters were projected to EPSG:9784 and processed in ArcGIS 10.3 (extraction, resampling, mosaicking, and masking). Soil information was obtained from the FAO map catalogue and the USDS NRCS SSURGO database. Following watershed delineation, LULC, soil raster, and slope (derived from DEM) were overlaid to generate Hydrologic Response Units (HRUs)—spatially homogeneous units defined by land cover, soil, and slope [67,68]. Reservoir data were compiled from the Alabama Reservoir Outdoor database, and the observed streamflow records were collected from the USGS National Water Information System. A summary of all datasets, variables, and software tools is provided in Table 1.

Table 1. Data sources used in this study, including spatial datasets, climate variables, and hydrologic inputs.

Data	Sources	Types
Climate data	From NASA website: (https://power.larc.nasa.gov/data-access-viewer/, accessed on 1 January 2025)	(i) Solar Radiation; (ii) Humidity; (iii) Wind; (iv) Rainfall; (v) Temperature.
LULC	National Land Cover Database (NLCD): https://www.sciencebase.gov/catalog/item/6345b637d34e342aee0863aa, accessed on 1 January 2025	Years: 1992; 2011; 2021
DEM	USGS Earth Explorer	SRTM 1 arc second; 30 m × 30 m resolution.
Soil shapefile	FAO Map Catalog: https://www.fao.org/soils-portal/data-hub/soil-maps-and-databases/faounesco-soil-map-of-the-world/en/, accessed on 1 January 2025	Different soil types with associated chemical and textural properties
	Soil Survey Geographic (SSURGO): https://nrcs.app.box.com/v/soils/folder/233398887779, accessed on 1 January 2025	
Cross dam information	Reservoirs | Outdoor Alabama: https://www.outdooralabama.com/wherefish-alabama/reservoirs, accessed on 1 January 2025	Reservoir capacity, discharge, primary spillway.
Lithological shapefile	Geological Survey of Alabama (GSA): https://www.gsa.state.al.us/gsa/groundwater/assessment, accessed on 1 January 2025	Different lithological formations exposed on the surface.
Stream flow/ Monitoring points	USGS Current Water Data for the Nation (River discharge in meter cube per second): https://waterdata.usgs.gov/al/nwis/wu, accessed on 1 January 2025	Stations: M1—USGS 02433496; M2—USGS 02433500; M3—USGS 02437100; M4—USGS 02441390; M5—USGS 02448500; M6—USGS 02447025; M7—USGS 02448900; M8—USGS 02467000; M9—USGS 02469761; M10—USGS 02453500; M11—USGS 02465000; M12—USGS 02398300; M13—USGS 02399200; M14—USGS 02397530; M15—USGS 02400100; M16—USGS 02407000; M17—USGS 02414500, M18—USGS 02414715; M19—USGS 02419890; M20—USGS 02420000; M21—USGS 02428400 (Figure 1a)

4. Methodology

To evaluate the impacts of human intervention and climatic change, multiple models were developed using ArcSWAT (a long term, large-scale, process based and semi-

distributed watershed model) following a structured sequence of steps (Figure 5). The multi-model strategy reduces uncertainty through comparison.

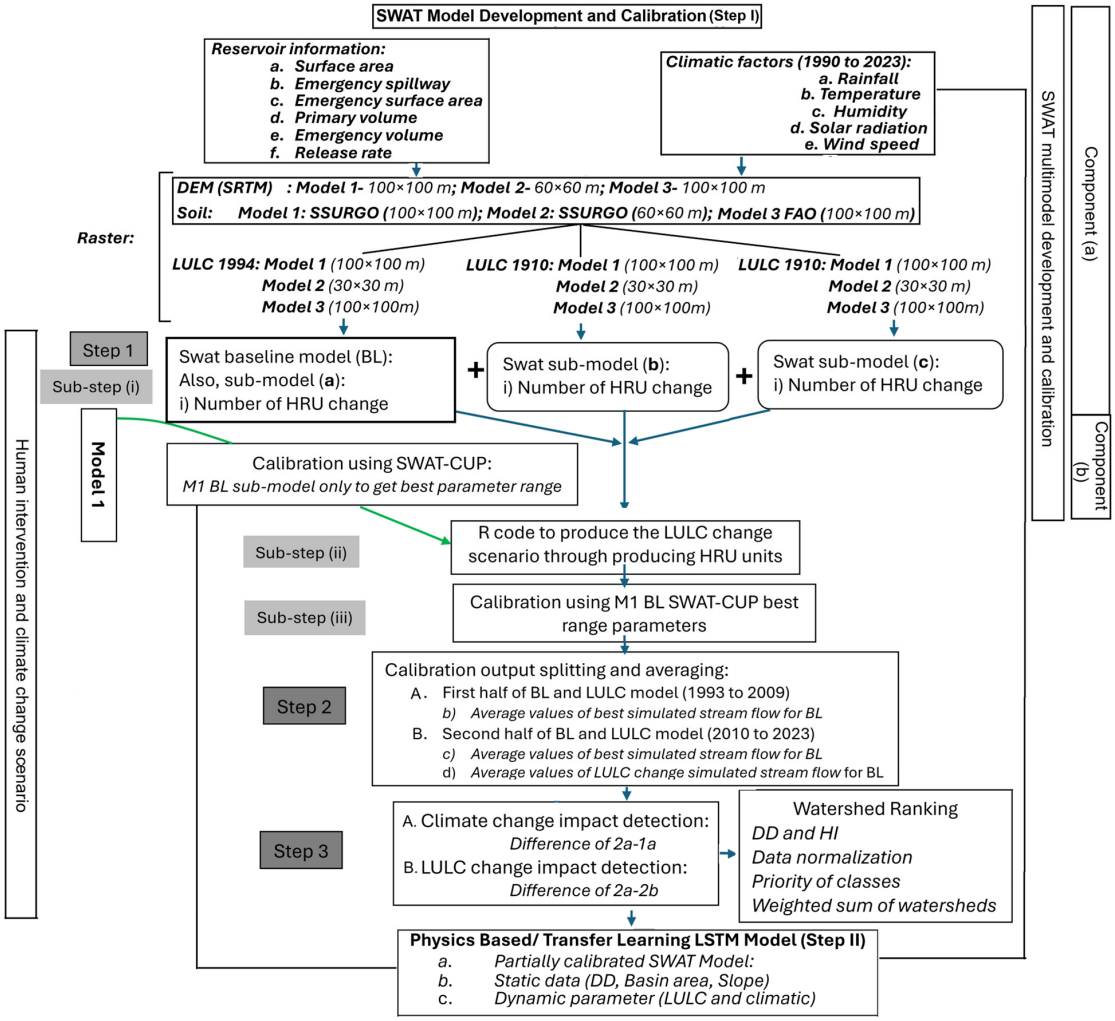

Figure 5. Workflow for assessing LULC and climate variability impacts. **Step I:** SWAT model development—build, calibrate, and validate the baseline model (M1), then construct two LULC submodels (2010 and 2021) and quantify LULC change impacts using the R script (https://github.com/tamnva/SWAT_LUC accessed on 1 January 2025). LULC models are calibrated with the best-fit parameters from M1. **Interim:** Perform watershed vulnerability ranking based on SWAT outputs. **Step II:** Physics-informed ML development—train an LSTM model using SWAT outputs and static/dynamic predictors to refine simulations. **Step 1:** Develop/calibrate/validate BL (M1) and LULC submodels. **Step 2:** Partition the simulation period into 1993–2009 and 2010–2023. **Step 3:** Integrate results to separate and assess the contributions of climate variability and LULC change.

In **Step I (a)**, we prepared required rasters and meteorological datasets for watershed delineation, characterization, and HRU development. Reservoir attributes, climate, lithology, and LULC inputs were incorporated to simulate hydrologic processes. In **Step I (b)**, we calibrated the model with SWAT-CUP, identifying influential streamflow parameters and iteratively adjusting their ranges to improve agreement with observations.

In **Step II**, we applied a physics-informed transfer-learning LSTM (a recurrent neural network) to enhance performance by integrating partially calibrated SWAT outputs with static and dynamic predictors. Model skill was evaluated using Nash–Sutcliffe Efficiency (NSE). We then conducted scenario analysis comparing the baseline (BL) model to two LULC-based submodels (Figure 5), followed by watershed vulnerability ranking using a multi-criteria framework.

4.1. SWAT Model Overview and Development of Multiple SWAT Models

SWAT is a long-term (e.g., 30 years here), process-based, semi-distributed model designed to simulate the environmental impacts of land use and climate change at daily or monthly time steps [69]. Detailed theoretical documentation is available in previous literature [70–72]. Land use and climate strongly influence water, sediment, and chemical yields, and SWAT provides insights into these processes through comprehensive water balance calculations. In both reservoir and watershed modeling, the water balance component—the main driver of SWAT—simulates the effects of hydrologic inputs and outputs on single plant growth [69]. To estimate sediment yield, SWAT incorporates the Modified Universal Soil Loss Equation (MUSLE) developed by Williams and Berndt [73]. Watershed hydrology in SWAT is represented in two phases: (1) the land phase, which generates water, sediment, nutrient, and pesticide loads within each sub-basin, and (2) the routing (or stream) phase, which governs the transport of these loads through the channel network to the watershed outlet [69].

For this study, three major SWAT models—M1, M2, and M3—were developed by keeping the initial 3-year warmup period. Each model includes three sub-models based on LULC scenarios: (a) the baseline (BL) scenario, (b) a 2011 LULC-based sub-model, and (c) a 2021 LULC-based sub-model. The sub-models were constructed using LULC maps from 1992, 2011, and 2021, respectively, to generate distinct HRUs as indicated in Figure 5, **sub-step (i) of Step 1**. The grid sizes and raster sources for each model are summarized in Table 2. This design facilitates evaluation of how input resolution and data origin influence hydrologic simulation results identified before [64]. To manage HRU complexity and ensure efficient model performance, thresholds were applied for land use (15%), soil (5%), and slope (10%), consistent with values reported in prior studies [10,74,75]. Slope classes were defined as follows: for M1 and M3—0–20°, 20–40°, 40–60°, and 60–91°; for M2—0–30°, 30–60°, 60–90°, and 90–120°. These ranges follow Ougahi et al. [76].

Table 2. Input parameters and grid sizes for three SWAT models (M1, M2, and M3) and parameter settings for the ML model. The digital elevation model (DEM) data are from SRTM, obtained via the USGS Earth Explorer portal. Soil source for each model: M1: SSURGO (NRCS; full coverage); M2: SSURGO (NRCS; full coverage); and M3: FAO global soil raster (18 classes). STATSGO was evaluated as a potential fallback during preprocessing but was not used, because SSURGO provided complete coverage of the study area.

Layer	Parameters	M1		M2		M3	
		BL Model	**LULC Model**	**BL Model**	**LULC Model**	**BL Model**	**LULC Model**
DEM	Grid size: Source:	100 × 100 m (SRTM)	100 × 100 m (SRTM)	60 × 60 m (SRTM)	60 × 60 m (SRTM)	100 × 100 m (SRTM)	100 × 100 m (SRTM)
LULC	Grid size: Source:	100 × 100 m (NLCD)	100 × 100 m (NLCD)	30 × 30 m (NLCD)	30 × 30 m (NLCD)	100 × 100 m (NLCD)	100 × 100 m (NLCD)
Soil	Grid size: Source:	100 × 100 m (SSURGO)	100 × 100 m (SSURGO)	100 × 100 m (SSURGO)	100 × 100 m (SSURGO)	100 × 100 m (FAO)	100 × 100 m (FAO)

Impacts of climate and land-use/land-cover (LULC) change on streamflow were evaluated for models M1–M3. Scenario 1 (baseline, BL) used LULC fixed at 1992 with long-term climate data; Scenario 2 used LULC from 1992, 2011, and 2021, with an R script producing the final HRUs. For each scenario, streamflow (SF) values were split into 1990–2009 and 2010–2023 and averaged (Figure 5, Step 2). Climate- and LULC-related SF effects were isolated by subtraction (Figure 5, Steps 3A and 3B). This multi-model framework enables comparisons across models and validation against observed runoff.

4.2. Machine Learning Model (LSTM) Development Using Transfer Learning

LSTM networks are widely used for sequential data and were designed to overcome the vanishing-gradient limitations of standard RNNs. Each LSTM unit contains a memory cell and three gates—input, forget, and output—that regulate information flow by deciding what to write, what to erase, and what to expose. The input gate admits relevant information to update the cell state, the forget gate discards unnecessary information, and the output gate determines what information is passed to the next step. To improve runoff simulation accuracy—particularly for peak flows—partially calibrated monthly outputs from SWAT were integrated into a machine learning (ML) model [77]. The objective was to compare the performance of SWAT and ML approaches and to identify key input features influencing runoff. Transfer learning was employed to leverage the process-based strengths of SWAT while enhancing predictive accuracy through data-driven methods.

The ML model employed a relatively simple architecture with an output size of 1, hidden size of 128, batch size of 28, and three layers. Sequence lengths were set to 5 for W4, 8 for W19, and 4 for the remaining watersheds. We trained the models with the Adam optimizer and tuned hyperparameters to their optimal values. Data was partitioned into 80% for training, 10% for testing, and 10% for validation.

Input rationale and hydrologic justification: The current study grouped ML predictors into four hydrologically motivated sets: (i) static physiography—area, mean slope, and mean elevation—to constrain storage, drainage potential, and baseline runoff propensity; (ii) dynamic climate—monthly precipitation and temperature—to drive seasonality and interannual variability; (iii) dynamic land surface—monthly watershed LULC fractions—to reflect gradual shifts in infiltration and runoff generation; and (iv) a physics-informed predictor—partially calibrated SWAT-simulated runoff—to inject process structure via transfer learning, which stabilizes learning and helps correct residual biases, particularly around peak flows. This architecture was selected to balance computational efficiency with sufficient complexity to capture temporal dependencies in hydrological data.

4.3. Multi-Model Calibration, Validation, Uncertainty, and Sensitivity Analysis Using SWAT-CUP

Model calibration and validation are critical—but often challenging—steps in hydrologic modeling, particularly when model results are used to inform decision-making [13,78–80]. Calibration outcomes are influenced by model uncertainty, which arises from model conceptualization, parameter selection, and methodological approach. This uncertainty can be quantified using global sensitivity functions and variance-based methods [81,82]. Calibration with SWAT-CUP is a semi-automated process in which parameter values and ranges are manually refined and progressively narrowed through multiple rounds of iterative adjustments between automatic calibration runs [9,83]. In this study, however, separate calibration for each LULC-based model did not yield significant differences in performance.

Among the three models, M1 was selected for full calibration and validation. A total of 38 parameters were adjusted, categorized as follows: groundwater (6), management (2), HRU (10), routing (2), basin (16), and soil (2). Based on Bauwe et al. [84], five iterations with 100 steps each were deemed sufficient to identify an optimal parameter set. The final calibrated parameters from M1 were applied to M2 and M3 for both BL and LULC change scenarios.

Model performance and watershed vulnerability were evaluated using four statistics: coefficient of determination (R^2), Nash–Sutcliffe efficiency (NSE; $\geq$0.50), percent bias (PBIAS; $\leq$15% considered satisfactory), and Kling–Gupta efficiency (KGE) [84,85]. These metrics are widely recommended for hydrologic model evaluation, with suitability thresh-

olds following Moriasi et al. [86]. For the ML model, NSE was also used as the primary evaluation metric.

Sensitivity analysis identifies influential parameters, improving calibration efficiency, refining uncertainty estimates, and enhancing overall model performance and robustness [69,81]. In this study, in addition to streamflow calibration and validation, sensitivity analysis was conducted using the SUFI-2 algorithm in SWAT-CUP [87]. Two statistical indicators were used during calibration: the *p*-value ($p < 0.05$ indicates higher sensitivity) and the *t*-statistic (larger absolute values indicate higher sensitivity) [81].

4.4. Parameters Regionalization

Parameter regionalization helps assess watershed homogeneity and enables hydrologic calibration in ungauged basins [88]. In this study, we used a mean-value approach, defining parameter ranges by averaging the minimum and maximum values from gauged watersheds [13]. These averaged ranges were applied in calibration tests, refined within stream sub-basins based on global performance metrics (e.g., NSE), and then transferred to ungauged basins.

4.5. Watershed Ranking (WR)

We applied the Analytical Hierarchy Process (AHP) and Principal Component Analysis (PCA), consistent with prior studies on groundwater potential and watershed prioritization [89–94]. In Alabama, the extensive reservoir network substantially modifies natural flow regimes and shapes regional hydrologic conditions.

To assess watershed vulnerability to streamflow, 35 watersheds were evaluated based on three categories of factors

- **Physical factors:** hypsometric index and drainage density
- **Dynamic factors:** LULC (water, urban, forest, grassland, agriculture), and streamflow (SF) for climate and LULC impacts
- **Static factor:** watershed area

Therefore, ranking was performed using Saaty's AHP method [95,96], which assigns a priority scale from 1 (highest) to 14 (lowest), as formalized in Equation (1).

To ensure a consistent comparison across watersheds, all input factors were normalized by unit area using the following equations:

$\text{Water}_{(i = 1 \text{ to } 14)} = \text{Water}^i / \text{Area}^i$;

$\text{Urban}_{(i = 1 \text{ to } 14)} = \text{Urban}^i / \text{Area}^i$;

$\text{Forest}_{(i = 1 \text{ to } 14)} = \text{Forest}^i / \text{Area}^i$;

$\text{Grass}_{(i = 1 \text{ to } 14)} = \text{Grass}^i / \text{Area}^i$;

$\text{Agriculture}_{(i = 14 \text{ to } 1)} = \text{Agriculture}^i / \text{Area}^i$;

$\text{LULC change SF}_{(i = 14 \text{ to } 1)} = \text{LULC Change SF}^i / \text{Area}^i$;

$\text{Climate change SF}_{(i = 14 \text{ to } 1)} = \text{Climate change SF}^i / \text{Area}^i$.

The watershed ranking index, WR^i, was calculated using a priority-based weighted summation, as expressed in Equation (1):

$$\begin{aligned} \mathbf{WR^i} = & \left(\frac{P^i_{HI\ (i=\ 14\ to\ 1)}}{\sum_1^{14} P^i_{HI\ (i=\ 14\ to\ 1)}} \times 14\right) + \left(\frac{P^i_{DD\ (i=14\ to\ 1)}}{\sum_1^{14} P^i_{DD\ (i=14\ to\ 1)}} \times 14\right) + \left(\frac{P^i_{Water\ (i=1\ to\ 14)}}{\sum_1^{14} P^i_{Water\ (i=1\ to\ 14)}} \times 14\right) + \left(\frac{P^i_{Urban\ (i=1\ to\ 14)}}{\sum_1^{14} P^i_{Urban\ (i=14\ to\ 1)}} \times 14\right) + \\ & \left(\frac{P^i_{Forest\ (i=1\ to\ 14)}}{\sum_1^{14} P^i_{Forest\ (i=14\ to\ 1)}} \times 14\right) + \left(\frac{P^i_{Grass(i=1\ to\ 14)}}{\sum_1^{14} P^i_{Grass\ (i=14\ to\ 1)}} \times 14\right) + \left(\frac{P^i_{Agriculture(i=14\ to\ 1)}}{\sum_1^{14} P^i_{Agriculture(i=14\ to\ 1)}} \times 14\right) + \\ & \left(\frac{P^i_{LULC\ change\ SF\ (i=14\ to\ 1)}}{\sum_1^{14} P^i_{LULC\ change\ SF\ (i=14\ to\ 1)}} \times 14\right) + \left(\frac{P^i_{Climate\ change\ SF\ (i=14\ to\ 1)}}{\sum_1^{14} P^i_{Climate\ change\ SF\ (i=14\ to\ 1)}} \times 14\right) \end{aligned} \quad (1)$$

where i is the watershed index (1 to 14); $P_x(i)$ is the priority value for factor x at watershed i (ranging from 1 to 14; 1 = highest priority); and x represents the nine factors: HI, DD, Water,

Urban, Forest, Grass, Agriculture, LULC Change SF, and Climate Change SF. Notes: (i) For positively correlated factors (e.g., Water, Forest), lower values are prioritized (ranking from 1 to 14). (ii) For negatively correlated factors (e.g., Agriculture, SF impacts), higher values are prioritized (ranking from 14 to 1). (iii) The index aggregates all weighted priority scores to produce a final watershed ranking.

WR^i Range and Vulnerability Classes: WR^i ranged from 1.20 to 16.80 (range = 15.60) and was divided into five equal intervals of 3.12:

- 1.20–4.32: Very High Vulnerability
- 4.32–7.44: High Vulnerability
- 7.44–10.56: Moderate Vulnerability
- 10.56–13.68: Low Vulnerability
- 13.68–16.80: Very Low Vulnerability

Effects on Streamflow: High drainage density and hypsometric integral increase runoff by reducing infiltration. In contrast, greater coverage of water bodies and forests decrease runoff by enhancing water storage and infiltration. Urbanization generally increases runoff by reducing infiltration, thereby degrading streamflow regimes. In our prioritization framework, this is treated as a negative impact.

Impact on Dissolved Load: Increases in streamflow driven by climate or LULC changes negatively affect chemical transport. In Equation 1, factors that increase SF are assigned negative values; consequently, larger negative values indicate higher vulnerability, and the corresponding priority (p) values are reversed.

5. Results

5.1. LULC and Climatic Change Scenario

Changes in vegetation cover, temperature, precipitation patterns, and atmospheric CO_2 collectively alter both surface- and groundwater-fed hydrology [31]. Of the five land-cover classes considered, water bodies, urban areas, and grasslands increased across all watersheds between 1992 and 2021, whereas forest and agricultural land declined (Table S4). Average annual rainfall ranged from 1314 to 1573 mm during 1990–2009 (Figure S2a) and from 1290 to 1623 mm during 2010–2023 (Figure S2b), with higher totals in the northwest that gradually decreased toward the south. The spatial difference between the two periods (Figure S2c) shows the largest decrease in the east (~−91 mm) and the greatest increase in the north (~+105 mm), with most areas changing within −50 to +50 mm. Overall, the Alabama watershed exhibited signs of rainfall deficit, whereas the upper Black Warrior watershed showed increasing rainfall over time.

5.2. Model Calibration, Validation, and Uncertainty

5.2.1. SWAT Model

SWAT results show that HRU counts varied across the baseline (LULC 1992), the LULC-2011 and LULC-2021 cases, and the scenarios. In that order, the HRU counts were: M1 = 108, 78, 91, 110; M2 = 107, 77, 88, 109; and M3 = 194, 139, 162, 195 (Table 2). This variation reflects sensitivity to input-data configuration and source selection [64]. In general, a higher number of HRUs improves spatial detail and representation of watershed heterogeneity but increases model complexity and computational cost.

SWAT-CUP was used to calibrate the SWAT model against observed streamflow. Several calibration–validation split strategies exist [81,97–99]; here we adopted a two-thirds split, consistent with prior applications (e.g., Daggupati et al. [99]) for climate and land-use change evaluations. Calibration/validation summary (text synopsis of Table S5): across gauges and models (M1–M3), calibration skill is generally good to very good (NSE and R^2), with validation remaining satisfactory to good and only a few outliers at specific

stations. KGE shows a similar pattern, and PBIAS is typically within ±15%, indicating limited systematic bias. These results are consistent across the three basins, with expected site-to-site variability related to reservoir influences, data gaps, and local heterogeneity. Full station-level values are provided in Table S5 (Supplementary Materials).

Compared with prior studies at other sites, our calibration/validation results show higher R^2 and NSE than typical daily time-step performance (previous ranges: 0.40–0.80 for R^2 and 0.50–0.80 for NSE) [100] and are close to reported monthly results (0.88/0.85 for R^2 and 0.85/0.84 for NSE, respectively) [101], indicating reliable model performance. The watersheds in Table S5 were selected for their complete, quality-controlled streamflow records of sufficient length to support robust calibration/validation and to span the three basins and major physiographic settings. Watersheds with incomplete or inconsistent records were excluded from this summary but are included in the broader multi-model analyses.

Figure S3a–c in the Supplementary Material present the calibration and validation plots for M1, plotted on a 2000 m^3/s scale.

5.2.2. ML Model

Incorporating partially calibrated streamflow along with static and dynamic parameters substantially improved model performance, with most NSE values exceeding 0.85. However, stations W13, W17, W19, and W27 showed lower NSE values (0.78, 0.66, 0.72, and 0.73, respectively; Table S5). These localized discrepancies likely reflect watershed-specific heterogeneity and data limitations that can reduce transfer-learning efficiency. Similar station-specific accuracy reductions have been reported for transfer-learning LSTM models in groundwater-level simulation [33]. Figures S4a (Tombigbee River Basin) and S4b–S4c (Black Warrior and Alabama–Tallapoosa basins) present comparative calibration, validation, and prediction results for the ML model.

5.3. Model Sensitivity Analysis

Of the 38 parameters tested, 21 were identified as sensitive ($p < 0.05$) across the calibrated watersheds using SWAT-CUP (Table S6a for M1). The most frequently sensitive were TRNSRCH (13 watersheds), CH_N2 (10), SURLAG, ALPHA_BF, and CN2 (5 each), GWQMN and CH_K2 (4 each), and ESCO (3). The remaining 13 parameters were sensitive in only one or two watersheds. Overall, groundwater and channel-routing parameters exert the strongest influence on watershed-scale hydrologic responses.

Table S6a shows that ten parameters in W27 were sensitive across four scenarios: (a) full calibration (1993–2023), (b) calibration (1993–2009), (c) validation (2010–2023), and (d) LULC change (1993–2023). A comparative analysis of sensitive parameters for M2 and M3 is provided in Table S6b (Supplementary Materials). The best-fit values for the 21 sensitive M1 parameters after five calibration iterations are listed in Table S7. Overall, changes in grid size and soil-data source slightly altered the set of sensitive parameters and their ranges, primarily due to shifts in HRU distribution and watershed area. In practice, using higher-resolution soil data (e.g., SSURGO) is recommended to improve calibration reliability and better capture hydrologic variability across watersheds.

We highlight W4, W13, W16, W17, W19, W26 and W27 as illustrative examples because they exhibited the largest counts or widest ranges of sensitive parameters across scenarios; results for all other watersheds (with fewer or less variable sensitive parameters) are fully reported in Table S6a.

5.4. Parameter Globalization

Using average parameter values from W4 and W6 reproduced W4 reasonably well (NSE = 0.56) but not W6 (Figure 1a). In the Black Warrior Basin, averaging parameters from W8 (NSE = 0.54) and W16 did not transfer well to W16 (NSE = 0.43), underscoring

limits to parameter transferability. By contrast, the averaging approach performed better in the Alabama and Tallapoosa basins. Table S8 reports transfer metrics across the three major basins.

Validity assessment for ungauged applications: the current study assessed the transferability of "globalized" parameters by benchmarking against adjacent gauged donor basins (immediately upstream and/or downstream; see Figure 1a). For each ungauged/target basin we (i) averaged donor parameter sets, (ii) simulated with the transferred set, and (iii) evaluated performance using NSE, R^2, KGE, and PBIAS as described in Section 4.3 for the accepted range. This procedure yielded W6 = 0.76 when averaging W4–W9, W26 = 0.65 from W20–W31; and W27 = 0.67 from W17–W28 (Figure 1a), whereas transfer to W16 remained weak (NSE = 0.43), reflecting reservoir and land-use heterogeneity. These benchmarks (see Table S5 and examples discussed above) support the method's use while also delineating its limits, which motivates our multi-model and vulnerability-ranking framework.

On the magnitude of NSE under transfer: the NSE values reported in this subsection arise from parameter-transfer tests for ungauged basins, not full calibrations; accordingly, acceptance targets are lower than for gauged sites. We therefore judge performance using a satisfactory band for monthly flows ($\approx$NSE $\geq$ 0.50) and corroborate R^2, KGE, and PBIAS. In practice, transferred runs typically achieve ~0.50–0.65 (e.g., W6 = 0.76 when averaging W4–W9), which is consistent with regionalization practice and sufficient for screening and ranking in our workflow, while full calibration results remain reported elsewhere in the paper and Supplementary Materials. The holistic scenario can be found from Figure 1a for watershed distribution; (e.g., W4–W6–W9; W17–W23/25–W28; W20–W26–W31); Figure S3a–c for calibration and validation; Table S7 for the calibrated BL parameter set that is averaged/transferred in the tests; Table S5 for gauge-wise calibration/validation metrics (NSE, R^2, KGE, PBIAS) used to judge transfer performance (e.g., W6 $\rightarrow$ 0.76; W26 $\rightarrow$ 0.65; W27 $\rightarrow$ 0.67).

5.5. Evaluation of Human and Climate Impacts

The overall workflow is shown schematically in Figure 5 (Steps 1–3) using a multi-model approach aimed at reducing model uncertainty. Results are presented in the next section, with a comparative summary in Figure S5 (Supplementary Materials).

5.5.1. Average Streamflow Scenarios for the First Half of the Simulation Period (1993 to 2009): BL vs. LULC Models

- **BL Model**

Across all three basins, streamflow estimates from M1, M2, and M3 showed some variability in response to climatic changes. The Tombigbee Basin exhibited moderate variation in watersheds W6 and W31, likely reflecting their reservoir influence and geomorphic setting. In contrast, Black Warrior and Alabama Basins remained relatively consistent across models, with minor differences (Table 3). These results suggest that the Tombigbee Basin is more sensitive to climate variability than the Black Warrior and Alabama Basins.

- **LULC Change Model**

Model outputs revealed more pronounced variability in streamflow across all watersheds, particularly in the Tombigbee Basin. Comparisons among M1, M2, and M3 showed that LULC evolution amplified streamflow differences in certain sub-basins (e.g., W31 and W28), while others remained relatively stable. Detailed results are provided in Table 3. These findings highlight that LULC change exerts a stronger influence on streamflow variability than climate alone in some basins, implying the need to integrate land-use planning into watershed management strategies.

Table 3. Comparison of observed and simulated streamflow (SF) for two periods to assess the impacts of LULC and climate variability.

Basin	Watershed No.	Periods	OBS SF (m^3/s)	BL			LULC Related			Rainfall (mm)
				M1 (m^3/s)	M2 (m^3/s)	M3 (m^3/s)	M1 (m^3/s)	M2 (m^3/s)	M3 (m^3/s)	
Tombigbee Basin	4	1993–2010 Avg.	55	57	50	57	56	53	57	120
		2010–2022 Avg.	50	61	54	61	84	53	83	123
		Total Avg.	52	59	52	59	70	53	70	122
	6	1993–2010 Avg.	112	122	110	117	124	116	127	111
		2010–2022 Avg.	104	111	99	107	96	69	79	116
		Total Avg.	108	116	104	112	110	92	103	113
	9	1993–2010 Avg.	208	220	220	220	243	228	243	117
		2010–2022 Avg.	161	193	193	193	155	152	155	112
		Total Avg.	184	206	206	206	199	190	199	115
	19	1993–2010 Avg.	48	59	53	55	62	60	62	115
		2010–2022 Avg.	52	60	54	56	33	47	48	121
		Total Avg.	50	59	53	55	47	53	55	118
	20	1993–2010 Avg.	320	340	351	353	389	368	356	111
		2010–2022 Avg.	300	341	352	354	286	301	334	112
		Total Avg.	310	340	352	354	337	335	345	112
	31	1993–2010 Avg.	791	953	791	893	1077	948	932	113
		2010–2022 Avg.	864	1010	864	944	809	1005	930	110
		Total Avg.	828	981	828	919	943	977	931	111
Black Warrior Basin	8	1993–2010 Avg.	85	87	89	86	83	89	73	120
		2010–2022 Avg.	96	99	99	97	101	90	143	121
		Total Avg.	91	93	94	92	92	89	108	120
	16	1993–2010 Avg.	229	252	247	256	291	291	252	119
		2010–2022 Avg.	245	284	278	290	225	189	327	119
		Total Avg.	237	268	262	273	258	240	290	119
	26	1993–2010 Avg.	703	776	785	771	861	839	771	109
		2010–2022 Avg.	659	779	789	770	629	660	783	108
		Total Avg.	681	777	787	770	745	749	777	108
Tallapoosa and Alabama Basin	13	1993–2010 Avg.	70	74	73	75	75	81	81	111
		2010–2022 Avg.	71	76	74	76	71	46	61	117
		Total Avg.	71	75	74	75	73	64	71	114
	17	1993–2010 Avg.	90	84	84	93	85	85	85	117
		2010–2022 Avg.	81	87	87	95	76	46	76	120
		Total Avg.	86	85	85	94	80	66	80	119
	27	1993–2010 Avg.	167	166	177	165	179	177	186	120
		2010–2022 Avg.	175	168	180	167	149	79	116	123
		Total Avg.	171	167	178	166	164	128	151	122
	28	1993–2010 Avg.	571	703	701	680	779	808	793	124
		2010–2022 Avg.	668	743	742	720	584	543	575	119
		Total Avg.	620	723	722	700	682	676	684	121
	32	1993–2010 Avg.	817	831	833	832	978	1065	889	120
		2010–2022 Avg.	830	843	845	841	736	612	882	117
		Total Avg.	824	837	839	837	857	839	885	118

5.5.2. Average Streamflow Scenarios for the Second Half of the Simulation Period (2010–2023): BL and LULC Models

- **BL model**

In the Tombigbee Basin, M1 and M3 produced similar streamflow values, whereas M2 estimated slightly lower flows for most watersheds. In the Black Warrior Basin, results were consistent between M1 and M2, while greater variability was observed in M3. For the Alabama Basin, flow patterns were largely comparable across models, with only minor differences in magnitude. Overall, M2 tended to underestimate flows, while M3 exhibited greater variability, highlighting differences in model sensitivity to climatic inputs.

- **LULC Change Model**

When LULC changes were incorporated, streamflow variability increased across all basins. In the Tombigbee Basin, M1 predicted the highest flows in several watersheds,

while M2 and M3 produced moderate to lower responses. In the Black Warrior Basin, notable differences emerged among models, particularly for M3. In the Alabama Basin, LULC changes resulted in pronounced shifts in streamflow values, especially under M2 and M3. Detailed streamflow values for all watersheds and models are provided in Table 3. Compared with the BL model results (fixed 1992 LULC), these findings demonstrate that LULC change introduces substantially greater variability among models than climate variability alone.

Therefore, average streamflow scenarios for both time-series halves highlights the role of land-use dynamics in watershed assessments and their influence on subsequent watershed vulnerability rankings.

Detailed streamflow values for all watersheds and models are presented in Table 3.

5.5.3. Average Rainfall Patterns in the Two Simulation Periods

In the **Tombigbee Basin**, average rainfall for 1990–2009 and 2010–2023 was assessed. Most watersheds showed modest increases between the two periods; only W9 declined (−5 mm). The corresponding watershed areas from W4 to W31 are 80, 2670, 5890, 3078, 4459, and 7877 km^2 (Table 3).

In the **Black Warrior Basin**, Table 3 summarizes average rainfall for the two periods (1990–2009 and 2010–2023). W8 and W26 declined by 10 mm and 1 mm, respectively, and the basin shows a slight downward trend overall. Watershed areas in this basin are 2556, 1170, and 2363 km^2.

In the **Alabama and Tallapoosa Basins**, W13 and W28 experienced reductions of 3 mm and 5 mm, respectively. Overall, the basins showed mixed but relatively modest changes, with slight decreases in some watersheds offset by small increases in others. The watershed areas considered in this basin are 3764, 1558, 3512, 928, and 2190 km^2.

Compared with the clearer increases observed in the Tombigbee Basin and the declines in the Black Warrior Basin, these results suggest that rainfall variability in the Alabama and Tallapoosa Basins has been more balanced and less directional. Consequently, streamflow responses in these basins are likely to remain relatively stable, with localized effects depending on watershed-specific conditions. Additionally, the Black Warrior Basin exhibits reduced inputs and heightened hydrologic stress. Overall, these results show that long-term rainfall trends and short-term averages do not always align, underscoring the complexity of climate–basin interactions.

5.5.4. Climate Variability Impact on Runoff

Table 4 shows the climate change and human impacted SF result. These results indicate that climate-driven streamflow responses revealed distinct spatial patterns. The Tombigbee Basin showed moderate variability, with certain watersheds more sensitive to rainfall changes. The Black Warrior Basin exhibited generally consistent increases across models, with only minor divergence. The Alabama Basin showed more uneven responses, with one watershed experiencing a large increase while most others showed small changes. Collectively, these findings underscore basin-specific sensitivities to climate variability, shaped by reservoir influence, land use, and geomorphic setting. These climate-only results provide a foundation for comparison with the subsequent LULC impact analysis, which further isolates the role of land-use change in shaping watershed responses.

Compared with climate-driven impacts, LULC changes exerted stronger and more spatially variable influences on streamflow across the three basins. While upstream watersheds showed relatively consistent behavior, downstream systems—particularly those with reservoirs or extensive land-use modifications—exhibited greater divergence among models. These results show the importance of accounting for human activities in watershed

assessments, as their impacts on runoff often exceed those of climate variability alone. To better quantify these differences, Section 5.7 below develops a watershed vulnerability ranking framework that integrates physical, static, and dynamic factors.

Table 4. LULC change and climate-related impacts on streamflow across 14 watersheds.

Watershed Name	W No.	LULC Changed SF (m^3/s): 2010 to 2023			Climate Variability SF (m^3/s): 1994 to 2023		
		M1	M2	M3	M1	M2	M3
Tombigbee Basin	**4**	23	−1	23	4	4	4
	6	−15	−31	−28	−10	−10	−10
	9	−37	−41	−38	−28	−28	−27
	19	−27	−8	−8	1	2	1
	20	−55	−51	−21	1	1	1
	31	−201	141	−13	57	73	50
Black Warrior Basin	**8**	3	−9	46	11	10	11
	16	−59	−88	38	32	31	34
	26	−150	−129	13	3	4	−1
Alabama and Tallapoosa Basin	**13**	−4	−29	−15	1	1	1
	17	−11	−41	−20	2	2	3
	27	−18	−101	−51	2	3	2
	28	−159	−199	−145	41	41	39
	32	−107	−234	40	11	13	9

5.6. Relationship Between Climate Change and Human Intervention (LULC Change)

Across all three basins, LULC change emerged as the dominant driver of streamflow variability, though the degree of influence varied among models. Climate variability played a secondary role, except in isolated cases within the Black Warrior Basin. The Alabama Basin showed the strongest dominance of LULC impacts, whereas the Black Warrior Basin exhibited the greatest relative sensitivity to climate variability. A detailed summary of proportional impacts is provided in Table S9 (Supplementary Materials, which summarizes cross-watershed sensitivity outcomes based on this SUFI-2 ($p < 0.05$, higher $|t|$) criterion). For dominance criterion, this study labels watershed impacts as **LULC-dominated** when the LULC contribution exceeds 60% in ≥2 of 3 models (M1–M3); **Climate-dominated** when the climate contribution exceeds 60% in ≥2 of 3 models; and **Both** when neither factor consistently exceeds 60% across models (i.e., mixed or model-dependent dominance). For model-agreement criterion, the inter-model agreement is classified as strong when the inter-model range of percentage contributions (M1–M3) is ≤15 percentage points (pp), moderate when it is >15–30 pp, and weak when it is >30 pp. This provides a consistent, quantitative basis for labeling agreement across models. These basin-level contrasts are directly reflected in the watershed vulnerability ranking results presented in the following section, which integrates physical, dynamic, and static factors to provide a comprehensive assessment.

5.7. Watershed Ranking (WR) Based on Impact

WR calculations indicate that streamflow—affected by static, dynamic, and human–climatic factors—exhibits mostly moderate vulnerability in its responses (Table 5).

A parallel assessment using a 1–7 scale with 0.5 intervals produced consistent results, confirming the robustness of the watershed priority ranking. The agreement between the two scales also indicates that the weighting approach within the AHP framework produced reliable results. Table 5 reports watershed-level vulnerability/priority scores computed with the AHP-weighted index (Equation (1)). Scores are shown on two equivalent scales (1–14 and 1–7 = ½ × [1–14]).

Table 5. Ranking of watershed vulnerability to human intervention and climate change. Includes both **1–14** and **1–7** scales (1–7 = ½ × [1–14]); **lower score = higher vulnerability**. Severity thresholds (1–14 scale): **High** $\leq$ **6.5**, **Moderate > 6.5–10.5**, **Low > 10.5.**.

Watershed No.	Priority for 1 to 14 Scale	Priority for 1 to 7 Scale	Severity
4	6.13	3.07	High
6	6.40	3.20	High
28	7.60	3.80	Moderate
16	7.73	3.87	Moderate
26	7.73	3.87	Moderate
9	8.27	4.13	Moderate
27	8.53	4.27	Moderate
19	9.20	4.60	Moderate
8	9.60	4.80	Moderate
20	9.60	4.80	Moderate
32	10.13	5.07	Moderate
31	11.33	5.67	Low
13	11.73	5.87	Low
17	12.00	6.00	Low

Interpretation of rankings: W4 and W6 ranked highest due to a combination of high drainage density, low hypsometric integral, and sensitivity to both climate variability and LULC change, making them particularly prone to rapid runoff responses. The moderate group includes watersheds where impacts were more mixed, often reflecting intermediate basin sizes or partial buffering by reservoirs. In contrast, watersheds classified as low vulnerability (e.g., W13, W17, W31) tend to have larger storage capacity, gentler slopes, or hydrological stability that reduces their sensitivity to short-term climatic and land-use fluctuations.

Management implications: These rankings provide a decision-support tool for prioritizing resource allocation. Watersheds in the high-vulnerability category (W4, W6) may require immediate attention for adaptive management, such as targeted land-use planning, reservoir operation strategies, or improved monitoring. Moderate-vulnerability watersheds could benefit from proactive measures to prevent escalation, while low-vulnerability systems can serve as comparative baselines for resilience studies.

6. Discussion

This study advances understanding of how human interventions and climate variability jointly influence watershed hydrology [84]. Climate variability associated with global warming alters rainfall patterns and, in turn, runoff dynamics. LULC change also exerts significant influence, with waterbody areas increasing across most watersheds—likely reflecting urban expansion that requires water storage [102] and agricultural water use. This study quantifies climate vs. LULC contributions via process-based counterfactuals (BL holds LULC fixed; LULC scenarios hold the climate period constant), which provides direct identification without assuming linear additivity. Standardized multiple regression is not used here, because monthly streamflow is nonlinear, autocorrelated, and reservoir-affected, and climate and LULC co-vary in space and time-conditions under which standardized partial coefficients can be unstable or misleading. Instead, we rely on (i) scenario contrasts summarized in Table S9, (ii) global sensitivity with SUFI-2 for SWAT parameters, and (iii) ML input checks (ablation/permutation), which better respect hydrologic process structure while yielding consistent conclusions about relative influence.

Model performance and sensitivity. Calibration results showed strong performance across most watersheds. For example, W8 achieved an NSE of 0.90 for the full simulation period (Table S5a), with 0.91 for 1993–2009 but a decline to 0.27 for 2010–2023. By contrast, M3 achieved an NSE of 0.96 (Table S5b), likely due to differences in grid resolution and input datasets (e.g., weather and LULC rasters), which affect streamflow representation and parameter sensitivity [101]. Other contributing factors may include missing observations or choices of raster ranges such as slope intervals and HRU definitions (Section 4.1). The main sensitive parameters included TRNSRCH, CH_N2, SURLAG, ALPHA_BF, CN2, GWQMN, CH_K2, and ESCO. Their hydrological roles are summarized as follows:

- **TRNSRCH**: Governs seepage from the streambed to groundwater; higher values increase losses, especially in permeable zones.
- **CH_N2**: Controls the main channel velocity via Manning's roughness; higher values simulate slower flow.
- **SURLAG**: Surface runoff lag time; lower values accelerate runoff response and advance peak-flow timing.
- **ALPHA_BF**: Baseflow response factor; lower values delay groundwater contributions.
- **CN2**: Curve number for runoff; higher values (urban areas) increase runoff, lower values (forests) enhance infiltration.
- **GWQMN**: Threshold aquifer water depth for baseflow; larger values delay baseflow onset.
- **CH_K2**: Channel seepage rate into aquifers; higher values increase infiltration losses.
- **ESCO**: Soil evaporation compensation factor; lower values allow deeper evaporation, altering soil moisture dynamics.

Heterogeneity and parameter globalization. The study area is highly heterogeneous, and average parameters did not adequately capture behavior across all watersheds (Section 5.4). Nonetheless, parameter globalization performed reasonably well in some downstream watersheds located close together, sometimes just one basin apart. Variability likely reflects lithological differences and complex topography, as the region lies within the southern Appalachian Mountains (Section 2).

Climate vs. LULC impacts. Streamflow responses to climate scenarios were consistent across models, largely due to uniform weather inputs and a fixed LULC map. By contrast, streamflow under human intervention scenarios varied significantly, primarily driven by differences in HRU counts (Section 5.2.1). Both climate and LULC change [103] affected streamflow across the two time periods, linked to altered rainfall patterns, expansion of water bodies, and declines in forest and grassland cover—all of which increase erosion and reduce the land's ability to retain runoff (Section 5.5). Because of these diverse LULC–soil combinations, HRU counts varied among sub-models, producing deviations in human-induced scenarios and confirming findings of prior studies [64,84]. The interaction between climate variability and human intervention impacts was further detailed in Section 5.6.

Implications. Integrating static, dynamic, and anthropogenic factors demonstrates that the models produced reliable results. Importantly, the watershed rankings (Section 5.7) capture these combined influences, highlighting vulnerable watersheds where runoff management is critical. The findings provide a decision-support framework for streamflow management strategies aimed at reducing pollutant transport from upland areas and improving resilience under changing climate and land-use conditions.

LSTM: Integrating the physics-informed LSTM with partially calibrated SWAT outputs improved skill at most gauges (NSE > 0.85) and reduced peak-flow bias by better capturing temporal dependencies in the rainfall–runoff signal; only a few sites (e.g., W13, W17, W19, W27) showed smaller gains, likely due to local heterogeneity and data gaps.

Comparison with previous studies. Previous hydrological research in Alabama and the broader southeastern U.S. has generally examined either climate variability or land-use

change in isolation, but rarely their combined impacts. For example, Gurung et al. [25] and Haas et al. [26] focused on uncontrolled watersheds. Our findings extend this body of work by systematically assessing both controlled and uncontrolled watersheds across three major basins in Alabama using a multi-model SWAT framework. By integrating process-based modeling with machine learning, the study improves predictive accuracy and highlights how basin-specific characteristics—such as lithology, reservoir presence, and LULC transitions—mediate hydrological responses. The watershed vulnerability ranking framework further advances prior approaches by offering a transferable method for prioritizing watershed management in data-scarce, human-modified regions.

7. Conclusions

This study applied an integrated hydrological modeling framework to evaluate watershed behavior and streamflow dynamics in Alabama under both climatic variability and land-use change. Using ArcSWAT with three multi-scale models (M1–M3), streamflow was simulated under baseline and LULC change scenarios from 1993 to 2023, with strong calibration performance (NSE = 0.91 for W4 in M1). Integration with an LSTM-based machine learning model further improved predictive accuracy, particularly under partially calibrated conditions. The findings provide practical insights for sustainable watershed management, water security, and ecosystem service protection, while also informing environmental policy in line with SDG (Sustainable Develipment Goals) 6 (Clean Water and Sanitation) and SDG 13 (Climate Action). Major findings of this study include:

(1) Drainage density generally exceeded 0.6 km/km^2, and hypsometric integral values were relatively high, although 10 of 35 watersheds had HI < 0.3, indicating spatial heterogeneity in erosional maturity.

(2) Rainfall trends revealed increasing climate variability and drought severity. Ten watersheds exhibited upward rainfall trends, while others declined. Three major droughts (1999–2003, 2006–2009, 2011–2013) were identified using SPI, with NASA POWER rainfall data showing good agreement with USGS records ($r \approx 0.7$).

(3) LULC changes (1992–2021) were marked by increases in waterbody, urban, and grassland areas and declines in forest and agricultural land, driving shifts in streamflow behavior.

(4) Soil data resolution strongly influenced HRU generation and streamflow results: 18 FAO soil classes and 5125 SSURGO soil classes produced notable differences across models.

(5) Sensitivity analysis identified 21 main parameters (out of 38), with routing (e.g., CH_N2), groundwater (e.g., ALPHA_BF, GWQMN), management (e.g., CN2), and HRU parameters (e.g., SURLAG) exerting the greatest influence on streamflow.

(6) Climate variability led to streamflow increases in most watersheds, except W6 and W9 (Tombigbee) and W26 (Black Warrior), which showed declines despite rainfall stability.

(7) LULC change exerted stronger and more spatially variable effects than climate alone, particularly in downstream watersheds influenced by reservoirs and land-use transitions. These findings show the importance of incorporating land-use dynamics into watershed assessments, as their impacts often outweigh those of climate variability when anthropogenic activities are considered.

(8) Vulnerability rankings classified W4 and W6 as highly vulnerable; ten watersheds as moderately vulnerable; and three as low vulnerability, reflecting greater resilience.

(9) Basin-level contrasts showed moderate climate sensitivity in the Tombigbee Basin, higher climate influence in parts of the Black Warrior Basin, and LULC-dominated impacts in the Alabama Basin.

(10) The SWAT–LSTM fusion consistently outperformed SWAT-only baselines, delivering higher NSE under partially calibrated conditions and more reliable peak-flow reproduction across heterogeneous basins, thereby improving predictive accuracy and robustness.

Overall, the results demonstrate that LULC change is the dominant driver of hydrological variability across Alabama, frequently outweighing climate effects. The integration of process-based SWAT modeling with machine learning enhances predictive robustness and captures basin-specific sensitivities shaped by lithology, reservoir operations, and land-use transitions. The proposed watershed vulnerability ranking framework offers a transferable decision-support tool for prioritizing management in data-scarce, human-modified regions. Collectively, these findings underscore the growing vulnerability of Alabama's river basins to combined climatic and anthropogenic pressures and highlight the need for proactive watershed and environmental management to sustain water resources, protect ecosystem services, and guide long-term policy.

Supplementary Materials: The following supporting information can be downloaded at: https://www.mdpi.com/article/10.3390/environments12100395/s1.

Author Contributions: Conceptualization, R.A. and Y.Z.; methodology, R.A., J.F., G.R.T. and Y.Z.; software, R.A.; validation, R.A.; formal analysis, R.A. and Y.Z.; investigation, R.A. and Y.Z.; resources, Y.Z.; data curation, R.A.; writing—original draft preparation, R.A., J.F., G.R.T., D.D.B., A.M.G. and Y.Z.; writing—review and editing, R.A., J.F., G.R.T., D.D.B., A.M.G. and Y.Z.; visualization, R.A.; supervision, Y.Z.; project administration, Y.Z.; funding acquisition, Y.Z. All authors have read and agreed to the published version of the manuscript.

Funding: This research was funded in part with federal funding from the Department of the Treasury under the Resources and Ecosystems Sustainability, Tourist Opportunities, and Revived Economies of the Gulf Coast States Act of 2012 (RESTORE Act). The statements, findings, conclusions, and recommendations are those of the authors and do not necessarily reflect the views of the Department of the Treasury or Alabama Department of Conservation and Natural Resources (ADCNR).

Data Availability Statement: The raw datasets supporting the conclusions of this study are available upon request.

Conflicts of Interest: Author Derek D. Bussan was employed by the company Derek Bussan's Consulting LLC, The remaining authors declare that the research was conducted in the absence of any commercial or financial relationships that could be construed as a potential conflict of interest.

References

1. Tian, H.; Xu, R.; Pan, S.; Yao, Y.; Bian, Z.; Cai, W.J.; Hopkinson, C.S.; Justic, D.; Lohrenz, S.; Lu, C.; et al. Long-term trajectory of nitrogen loading and delivery from Mississippi River basin to the Gulf of Mexico. *Glob. Biogeochem. Cycles* **2020**, *34*, e2019GB006475. [CrossRef]
2. Secchi, S.; Mcdonald, M. The state of water quality strategies in the Mississippi River Basin: Is cooperative federalism working? *Sci. Total Environ.* **2019**, *677*, 241–249. [CrossRef]
3. McIver, R.; Cullain, N.; Schmidt, A.L.; Lotze, H.K. Linking eutrophication indicators in eelgrass habitats to nitrogen loading and mitigating site characteristics in eastern New Brunswick, Canada. *Mar. Environ. Res.* **2019**, *144*, 141–153. [CrossRef]
4. Kronvang, B.; Andersen, H.E.; Børgesen, C.; Dalgaard, T.; Larsen, S.E.; Bøgestrand, J.; Blicher-Mathiasen, G. Effects of policy measures implemented in Denmark on nitrogen pollution of the aquatic environment. *Environ. Sci. Policy* **2008**, *11*, 144–152. [CrossRef]
5. Pieterse, N.M.; Bleuten, W.; Jørgensen, S.E. Contribution of point sources and diffuse sources to nitrogen and phosphorus loads in lowland river tributaries. *J. Hydrol.* **2003**, *271*, 213–225. [CrossRef]
6. Pott, C.A.; Fohrer, N. Best management practices to reduce nitrate pollution in a rural watershed in Germany. *Ambiente Agua Interdiscip. J. Appl. Sci.* **2017**, *12*, 888. [CrossRef]
7. Valayamkunnath, P.; Barlage, M.; Chen, F.; Gochis, D.J.; Franz, K.J. Mapping of 30-meter resolution tile-drained croplands using a geospatial modeling approach. *Sci. Data* **2020**, *7*, 257. [CrossRef] [PubMed]

8. Masud, M.A.A.; Samaraweera, H.; Mondol, M.M.H.; Septian, A.; Kumar, R.; Terry, L.G. Iron biochar synergy in aquatic systems through surface functionalities electron transfer and reactive species dynamics. *NPJ Clean Water* **2025**, *8*, 46. [CrossRef]
9. Mekonnen, Y.A.; Manderso, T.M. Land use/land cover change impact on streamflow using Arc-SWAT model, in case of Fetam watershed, Abbay Basin, Ethiopia. *Appl. Water Sci.* **2023**, *13*, 111. [CrossRef]
10. Maru, H.; Haileslassie, A.; Zeleke, T.; Teferi, E. Analysis of the impacts of land use land cover change on streamflow and surface water availability in Awash Basin, Ethiopia. *Geomat. Nat. Hazards Risk* **2023**, *14*, 1–25. [CrossRef]
11. Vandewiele, G.L.; Elias, A. Monthly water balance of ungauged catchments obtained by geographical regionalization. *J. Hydrol.* **1995**, *170*, 277–291. [CrossRef]
12. Bardossy, A. Calibration of hydrological model parameters for ungauged catchments. *Hydrol. Earth Syst. Sci. Discuss.* **2007**, *11*, 703–710. [CrossRef]
13. Gitau, M.W.; Chaubey, I. Regionalization of SWAT model parameters for use in ungauged watersheds. *Water* **2010**, *2*, 849–871. [CrossRef]
14. Kokkonen, T.S.; Jakeman, A.J.; Young, P.C.; Koivusalo, H.J. Predicting daily flows in ungauged catchments: Model regionalization from catchment descriptors at the Coweeta Hydrologic Laboratory, North Carolina. *Hydrol. Process* **2003**, *17*, 2219–2238. [CrossRef]
15. Bastola, S.; Ishidaira, H.; Takeuchi, K. Regionalization of hydrological model parameters under parameter uncertainty: A case study involving TOPMODEL and basins across the globe. *J. Hydrol.* **2008**, *357*, 188–206. [CrossRef]
16. Parajka, J.; Merz, R.; Blöschl, G. A comparison of regionalization methods for catchment model parameters. *Hydrol. Earth Syst. Sci.* **2005**, *9*, 157–171. [CrossRef]
17. Merz, R.; Blöschl, G. Regionalisation of catchment model parameters. *J. Hydrol.* **2004**, *287*, 95–123. [CrossRef]
18. McIntyre, N.; Lee, H.; Wheater, H.; Young, A.; Wagener, T. Ensemble predictions of runoff in ungauged catchments. *Water Resour. Res.* **2005**, *41*, W12434. [CrossRef]
19. Li, B.; Yang, L.; Song, X.; Diamantopoulos, E. Identifying surface water and groundwater interactions using multiple experimental methods in the riparian zone of the polluted and disturbed Shaying River, China. *Sci. Total Environ.* **2023**, *875*, 162616. [CrossRef]
20. Marcinkowski, P.; Piniewski, M.; Kardel, I.; Giełczewski, M.; Okruszko, T. Modelling of discharge, nitrate and phosphate loads from the Reda catchment to the Puck Lagoon using SWAT. *Ann. Wars. Univ. Life Sci. SGGW Land Reclam.* **2013**, *45*, 125–141. [CrossRef]
21. Yang, J.; Reicher, P.; Abbaspour, K.C.; Xia, J.; Yang, H. Comparing uncertainty analysis techniques for a SWAT application to the Chao he Basin in China. *J. Hydrol.* **2008**, *358*, 1–23. [CrossRef]
22. Abbaspour, K.C.; Yang, J.; Ivan, M.; Siber, R.; Bogner, K.; Mieleitner, J.; Zobrist, J.; Srinivasan, R. Modelling hydrology and water quality in the pre-alpine/alpine Thur watershed using SWAT. *J. Hydrol.* **2007**, *333*, 413–430. [CrossRef]
23. Faramarzi, M.; Abbaspour, K.C.; Schulin, R.; Yang, H. Modelling blue and green water resources availability in Iran. *Hydrol. Process* **2009**, *23*, 486–501. [CrossRef]
24. Schuola, J.; Karim, C.A.; Srinivasan, R.; Yang, H. Estimation of freshwater availability in the West African sub-continent using the SWAT hydrologic model. *J. Hydrol.* **2008**, *352*, 30–49. [CrossRef]
25. Gurung, D.P.; Githinji, L.J.M.; Ankumah, R.O. Assessing the nitrogen and phosphorus loading in the Alabama (USA) River Basin using PLOAD model. *Air Soil Water Res.* **2013**, *6*, 23–36. [CrossRef]
26. Haas, H.; Dosdogru, F.; Kalin, L.; Yen, H. Soft data in hydrologic modeling: Prediction of ecologically relevant flows with alternate land use/land cover data. *Water* **2021**, *13*, 2947. [CrossRef]
27. Abidin, R.Z.; Sulaiman, M.S.; Yusoff, N. Erosion risk assessment: A case study of the Langat Riverbank in Malaysia. *Int. Soil. Water Conserv. Res.* **2017**, *5*, 26–35. [CrossRef]
28. Dibaba, W.T.; Demissie, T.A.; Miegel, K. Watershed hydrological response to combined land use/land cover and climate change in highland Ethiopia: Finchaa catchment. *Water* **2020**, *12*, 1801. [CrossRef]
29. Tena, T.M.; Mwaanga, P.; Nguvulu, A. Impact of land use/land cover change on hydrological components in Chongwe River Catchment. *Sustainability* **2019**, *11*, 6415. [CrossRef]
30. Stuart, M.E.; Gooddy, D.C.; Bloomfield, J.P.; Williams, A.T. A review of the impact of climate change on future nitrate concentrations in groundwater of the UK. *Sci. Total Environ.* **2011**, *409*, 2859–2873. [CrossRef]
31. Jia, L.; Yen, N.; Pei, Y. A physics-coupled deep learning framework for hydrodynamic diffusion modeling in watershed systems: Integrating spatiotemporal networks and environmental constraints. *IEEE Access* **2025**, *13*, 34985–35003. [CrossRef]
32. Asadi, S.; Jimeno-Sáez, P.; López-Ballesteros, A.; Senent-Aparicio, J. Coupling SWAT+ with LSTM for enhanced and interpretable streamflow estimation in arid and semi-arid watersheds, a case study of the Tagus Headwaters River Basin, Spain. *Environ. Model. Softw.* **2025**, *186*, 106360. [CrossRef]
33. Rahman, A.T.M.S.; Sakib, S.M.; Reza, M.K.; Basak, A.; Hafiz, K.N.; Islam, M.S.; Hosono, T. Basin-wide groundwater level forecasting in Kumamoto, Japan: Integrating transfer learning with long short-term memory network. *Hydrol. Sci. J.* **2025**, *70*, 1–19. [CrossRef]

34. Gholizadeh, H.; Zhang, Y.; Frame, J.; Gu, X.; Green, C.T. Long short-term memory models to quantify long-term evolution of streamflow discharge and groundwater depth in Alabama. *Sci. Total Environ.* **2023**, *901*, 165884. [CrossRef]
35. Ghasemlounia, R.; Gharehbaghi, A.; Ahmadi, F.; Saadatnejadgharahassanlou, H. Developing a novel framework for forecasting groundwater level fluctuations using Bi-directional Long Short-Term Memory (BiLSTM) deep neural network. *Comput. Electron. Agr.* **2021**, *191*, 106568. [CrossRef]
36. Noori, N.; Kalin, L. Coupling SWAT and ANN models for enhanced daily streamflow prediction. *J. Hydrol.* **2016**, *533*, 141–151. [CrossRef]
37. KarimiDermani, B.; Green, C.T.; Tick, G.R.; Gholizadeh, H.; Wei, W.; Zhang, Y. Analyzing multi-year nitrate concentration evolution in Alabama aquatic systems using a machine learning model. *Environments* **2025**, *12*, 75. [CrossRef]
38. Oluwaniyi, O.; Zhang, Y.; Gholizadeh, H.; Li, B.; Gu, X.; Sun, H.; Lu, C. Correlating groundwater storage change and precipitation in Alabama, United States from 2000–2021 by Combining the water table fluctuation method and statistical analyses. *Sustainability* **2023**, *15*, 15324. [CrossRef]
39. Boumaiza, L.; Ammar, S.B.; Chesnaux, R.; Stotler, R.L.; Mayer, B.; Huneau, F.; Johannesson, K.H.; Levison, J.; Knöller, K.; Stumpp, C. Nitrate sources and transformation processes in groundwater of a coastal area experiencing various environmental stressors. *J. Environ. Manag.* **2023**, *345*, 118803. [CrossRef] [PubMed]
40. Smith, C.G.; Osterman, L.E.; Poore, R.Z. An examination of historical inorganic sedimentation and organic matter accumulation in several marsh types within the mobile bay and mobile—Tensaw River delta region. *J. Coast. Res.* **2013**, *63*, 68–83. [CrossRef]
41. Anderson, D.M.; Burkholder, J.M.; Cochlan, W.P.; Glibert, P.M.; Gobler, C.J.; Heil, C.A.; Kudela, R.; Parsons, M.L.; Rensel, J.E.; Townsend, D.W.; et al. Harmful algal blooms and eutrophication: Examining linkages from selected coastal regions of the United States. *Harmful Algae* **2008**, *8*, 39–53. [CrossRef]
42. Grabowska, M. The role of a eutrophic lowland reservoir in shaping the composition of river phytoplankton. *Ecohydrol. Hydrobiol.* **2012**, *12*, 231–242. [CrossRef]
43. ADECA; OWR. *Estimated 2015 Water Use and Surface Water Availability in Alabama*; Alabama Department of Economic and Community Affairs: Montgomery, AL, USA, 2015.
44. Vivoni, E.R.; Benedetto, F.D.; Grimaldi, S.; Eltahir, E.A.B. Hypsometric control on surface and subsurface runoff. *Water Resour. Res.* **2008**, *44*, W12502. [CrossRef]
45. Arefin, R.; Seker, D.Z.; Hore, R.; Meshram, S.G. GIS and remotely sensed data-based morphometric elements analysis for determination of Bengal Basin evolution. *Environ. Dev. Sustain.* **2024**, *26*, 3423–3456. [CrossRef]
46. Zuo, D.D.; Hou, W.; Zhang, Q.; Yan, P.C. Sensitivity analysis of standardized precipitation index to climate state selection in China. *Adv. Clim. Change Res.* **2022**, *13*, 42–50. [CrossRef]
47. Santos, J.F.; Portela, M.M.; Naghettini, M.; Matos, J.P.; Silva, A.T. Precipitation thresholds for drought recognition: A further use of the standardized precipitation index, SPI. *River Basin Manag.* **2013**, *172*, 3–14.
48. McKee, T.B.; Doesken, N.J.; Kleist, J. The relationship of drought frequency and duration to time scales. In Proceedings of the 8th Conference on Applied Climatology, Anaheim, CA, USA, 17–22 January 1993; American Meteorological Society: Boston, MA, USA, 1993.
49. WMO (World Meteorological Organization). *Standardized Precipitation Index User Guide, (WMO-No. 1090)*; World Meteorological Organization: Geneva, Switzerland, 2012.
50. Agnew, C.T. Using the SPI to identify drought. *Drought Netw. News* **2000**, *12*, 6–12.
51. Hayes, M.; Svoboda, M.; Wall, N.; Widhalm, M. The lincoln declaration on drought indices: Universal meteorological drought index recommended. *Bull. Am. Meteorol. Soc.* **2011**, *92*, 485–488. [CrossRef]
52. Sonali, P.; Kumar, D. Review of trend detection methods and their application to detect temperature changes in India. *J. Hydrol.* **2013**, *476*, 212–227. [CrossRef]
53. Kisi, O.; Ay, M. Comparison of Mann-Kendall and innovative trend method for water quality parameters of the Kizilirmak River, Turkey. *J. Hydrol.* **2014**, *513*, 362–375. [CrossRef]
54. Dabanlı, İ.; Şen, Z.; Yeleğen, M.; Şişman, E.; Selek, B.; Güçlü, Y. Trend assessment by the innovative-Şen method. *Water Resour. Manag.* **2016**, *30*, 5193–5203. [CrossRef]
55. Tabari, H.; Taye, M.T.; Onyutha, C.; Willems, P. Decadal analysis of river flow extremes using quantile-based approaches. *Water Resour. Manag.* **2017**, *31*, 3371–3387. [CrossRef]
56. Zhou, Z.; Wang, L.; Lin, A.; Zhang, M.; Niu, Z. Innovative trend analysis of solar radiation in China during 1962–2015. *Renew. Energy* **2018**, *119*, 675–689. [CrossRef]
57. Ahmas, I.; Zhang, F.; Tayyab, M.; Anjum, M.; Zamam, M.; Liu, J.; Farid, U.; Saddique, Q. Spatiotemporal analysis of precipitation variability in annual, seasonal and extreme values over upper Indus River basin. *Atmos. Res.* **2018**, *213*, 346–360.
58. Caloiero, T.; Coscarelli, R.; Ferrari, E. Application of the innovative trend analysis method for the trend analysis of rainfall anomalies in southern Italy. *Water Resour. Manag.* **2018**, *32*, 4971–4983. [CrossRef]

59. Kim, J.; Her, Y.; Bhattarai, R.; Jeong, H. Improving nitrate load simulation of the SWAT model in an extensively tile-drained watershed. *Sci. Total Environ.* **2023**, *904*, 166331. [CrossRef] [PubMed]
60. Paul, T.; Voicu, S. Image classification using machine learning algorithms in Google Earth Engine environment. *Inform. Econ.* **2021**, *25*, 5–16. [CrossRef]
61. Abburu, S.; Golla, S.B. Satellite image classification methods and techniques: A review. *Inter. J. Comput. Appl.* **2015**, *119*, 20–25. [CrossRef]
62. FAO. *Soil Map of the World*; United Nations Educational, Scientific, and Cultural Organization, UNESCO: Paris, France, 1981.
63. SoilGrids. An Automated System for Global Soil Mapping. Available online: http://soilgrids.org. (accessed on 1 April 2025).
64. Geza, M.; McCray, J.E. Effects of soil data resolution on SWAT model stream flow and water quality predictions. *J. Environ. Manag.* **2008**, *88*, 393–406. [CrossRef]
65. USDA. Natural Resources Conservation Services (NRCS). In *Soil Survey Geographic (SSURGO) Data Base: Data Use Information*; National Coil Survey Center: Lincoln, NE, USA, 1995.
66. Kroner, S.M.; Cozzie, D.A. *Data Collection for the Hazardous Waste Identification Rule, Section 7.0 Soil Data*; US Environmental Protection Agency Office of Solid Waste: Washington, DC, USA, 1999; p. 20460.
67. Arnold, J.G.; Fohrer, N. SWAT2000: Current capabilities and research opportunities in applied watershed modelling. *Hydrol. Process.* **2005**, *19*, 563–572. [CrossRef]
68. Behera, S.; Panda, R.K. Evaluation of management alternatives for an agricultural watershed in a sub-humid subtropical region using a physical process based model. *Agric. Ecosyst. Environ.* **2006**, *113*, 62–72. [CrossRef]
69. Arnold, J.G.; Moriasi, D.N.; Gassman, P.W.; Abbaspour, K.C.; White, M.J.; Srinivasan, R.; Santhi, C.; Harmel, R.D.; van Griensven, A.; Liew, M.W.V.; et al. SWAT: Model use, calibration, and validation. *Trans. ASABE* **2012**, *55*, 1491–1508. [CrossRef]
70. Arnold, J.G.; Srinivasan, R.; Williams, J.R. Large area hydrologic modeling assessment: Part 1 Model development. *J. Am. Water Resour. Assoc.* **1998**, *34*, 73–89. [CrossRef]
71. Gassman, P.W.; Reyes, M.R.; Green, C.H.; Arnold, J.G. The soil and water assessment tool: Historical development, applications, and future research directions. *Trans. ASABE.* **2008**, *50*, 1211–1250. [CrossRef]
72. Arnold, J.G.; Allen, P.M.; Volk, M.; Williams, J.R.; Bosch, D.D. Assessment of different representations of spatial variability on SWAT model performance. *Trans. ASABE* **2010**, *53*, 1433–1443. [CrossRef]
73. Williams, J.R.; Berndt, H.D. Sediment yield prediction based on watershed hydrology. *Trans. ASABE* **1977**, *20*, 1100–1104. [CrossRef]
74. Sisay, E.; Halefom, A.; Khare, D.; Singh, L.; Worku, T. Hydrological modelling of ungauged urban watershed using SWAT model. *Model. Earth Syst. Environ.* **2017**, *3*, 693–702. [CrossRef]
75. Zhang, Z.; Wu, M. Evaluating the transport and fate of nutrients in large scale river basins using an integrated modeling system. In *Landscape Ecology for Sustainable Environment and Culture*; Fu, B., Jones, K., Eds.; Springer: Dordrecht, The Netherlands, 2013. [CrossRef]
76. Ougahi, J.H.; Karim, S.; Mahmood, S.A. Application of the SWAT model to assess climate and land use/cover change impacts on water balance components of the Kabul River Basin, Afghanistan. *J. Water Clim. Change* **2022**, *13*, 3977–3999. [CrossRef]
77. Yang, S.; Tan, M.L.; Song, Q.; He, J.; Yao, N.; Li, X.; Yang, X. Coupling SWAT and Bi-LSTM for improving daily-scale hydro-climatic simulation and climate change impact assessment in a tropical river basin. *J. Environ. Manag.* **2023**, *330*, 117244. [CrossRef] [PubMed]
78. Migliaccio, K.W.; Chaubey, I. Multi-variable and multi-site calibration and validation of SWAT in a large mountainous catchment with high spatial variability. *Hydrol. Process.* **2007**, *20*, 1057–1073.
79. Trucano, T.G.; Swiler, L.P.; Igusa, T.; Oberkampf, W.L.; Pilch, M. Calibration, validation, and sensitivity analysis: What's what. *Reliab. Eng. Syst. Saf.* **2006**, *91*, 1331–1357. [CrossRef]
80. Daggupati, P.; Pai, N.; Ale, S.; Douglas-Mankin, K.R.; Zeckoski, R.W.; Jeong, J.; Parajuli, P.B.; Saraswat, D.; Youssef, M.A. A recommended calibration and validation strategy for hydrologic and water quality models. *Trans. ASABE* **2015**, *58*, 1705–1719. [CrossRef]
81. Abbaspour, K.C.; Rouholahnejad, E.; Vaghefi, S.; Srinivasan, R.; Yang, H.; Kløve, B. A continental-scale hydrology and water quality model for Europe: Calibration and uncertainty of a high-resolution large-scale SWAT model. *J. Hydrol.* **2015**, *524*, 733–752. [CrossRef]
82. Baroni, G.; Tarantola, S. A general probabilistic framework for uncertainty and global sensitivity analysis of deterministic models: A hydrological case study. *Environ. Model. Softw.* **2014**, *51*, 26–34. [CrossRef]
83. Farhad, M.; Mohsen, N.; Maryam, N. Application of SWAT model to simulate nitrate and phosphate leaching from agricultural lands to rivers. *Adv. Environ. Technol.* **2020**, *6*, 1–17.
84. Bauwe, A.; Kahle, P.; Lennartz, B. Evaluating the SWAT model to predict streamflow, nitrate loadings and crop yields in a small agricultural catchment. *Adv. Geosci.* **2019**, *48*, 1–9. [CrossRef]

85. Thavhana, M.P.; Savage, M.J.; Moeletsi, M.E. SWAT model uncertainty analysis, calibration and validation for runoff simulation in the Luvuvhu River catchment, South Africa. *Phys. Chem. Earth Parts A/B/C* **2018**, *105*, 115–124. [CrossRef]
86. Moriasi, D.N.; Arnold, J.G.; Liew, M.W.V.; Bingner, R.L.; Harmel, R.D.; Veith, T.L. Model evaluation guidelines for systematic 5quantification of accuracy in watershed simulations. *Trans. ASABE* **2007**, *50*, 885–900. [CrossRef]
87. Abbaspour, K.C.; Johnson, C.A. Estimating uncertain flow and transport parameters using a sequential uncertainty fitting procedure. *Vadose Zone J.* **2004**, *3*, 1340–1352. [CrossRef]
88. Dissanayake, D.M.K.P.; Wickramaarachchi, T.N. Parameter regionalization of semi-distributed hydrologic model for peak flow predictions in flood- prone monsoon-climate catchment in Sri Lanka. *Engineer* **2025**, *58*, 1–14. [CrossRef]
89. Arefin, R. Groundwater potential zone identification using an analytic hierarchy process in Dhaka City, Bangladesh. *Environ. Earth Sci.* **2020**, *79*, 268. [CrossRef]
90. Arefin, R. Groundwater potential zone identification at Plio-Pleistocene elevated tract, Bangladesh: AHP-GIS and remote sensing approach. *Groundw. Sustain. Develop.* **2020**, *10*, 100340. [CrossRef]
91. Rahaman, M.F.; Jahan, C.S.; Arefin, R.; Mazumder, Q.H. Morphometric analysis of major watersheds in Barind Tract, Bangladesh: A remote sensing and GIS-based approach for water resource management. *Hydrology* **2018**, *5*, 86–95. [CrossRef]
92. Rahaman, M.F.; Jahan, C.S.; Arefin, R.; Mazumder, Q.H. Groundwater potentiality study in drought prone barind tract, NW Bangladesh using remote sensing and GIS. *Groundw. Sustain. Develop.* **2019**, *8*, 205–215.
93. Jahan, C.S.; Rahaman, M.F.; Arefin, R.; Ali, S.; Mazumder, Q.H. Morphometric analysis and hydrological inference for water resource management in Atrai-Sib River Basin, NW Bangladesh using remote sensing and GIS technique. *J. Geol. Soc. India* **2018**, *91*, 613–620. [CrossRef]
94. Jahan, C.S.; Rahaman, M.F.; Arefin, R.; Ali, M.S.; Mazumder, Q.H. Delineation of groundwater potential zones of Atrai–Sib River basin in north-west Bangladesh using remote sensing and GIS techniques. *Sustain. Water Resour. Manag.* **2019**, *5*, 689–702. [CrossRef]
95. Saaty, T.L. A scaling method for priorities in hierarchical structures. *J. Math. Psychol.* **1977**, *15*, 234–281. [CrossRef]
96. Saaty, T.L. *The Analytic Hierarchy Process*; McGraw-Hill: New York, NY, USA, 1980; p. 278.
97. Klemeš, V. Operational testing of hydrological simulation models. *Hydrol. Sci. J.* **1986**, *31*, 13–24. [CrossRef]
98. Gan, T.Y.; Dlamini, E.M.; Biftu, G.F. Effects of model complexity and structure, data quality, and objective functions on hydrologic modeling. *J. Hydrol.* **1997**, *192*, 81–103. [CrossRef]
99. Daggupati, P.; Yen, H.; White, M.J.; Srinivasan, R.; Arnold, J.G.; Keitzer, C.S.; Sowa, S.P. Impact of model development, calibration and validation decisions on hydrological simulations in West Lake Erie Basin. *Hydrol. Process* **2015**, *29*, 5307–5320. [CrossRef]
100. Hassaballah, K.; Mohamed, Y.; Uhlenbrook, S.; Biro, K. Analysis of streamflow response to land use and land cover changes using satellite data and hydrological modelling: Case study of Dinder and Rahad tributaries of the Blue Nile (Ethiopia-Sudan). *Hydrol. Earth Syst. Sci.* **2017**, *21*, 5217–5242. [CrossRef]
101. Welde, K.; Gebremariam, B. Effect of land use land cover dynamics on hydrological response of watershed: Case study of Tekeze Dam watershed, northern Ethiopia. *Int. Soil. Water Conserv. Res.* **2017**, *5*, 1–16. [CrossRef]
102. Li, C.; Sun, G.; Caldwell, P.V.; Cohen, E.; Fang, Y.; Zhang, Y.; Oudin, L.; Sanchez, G.M.; Meentemeyer, R.K. Impacts of urbanization on watershed water balances across the conterminous United States. *Water Resour. Res.* **2020**, *56*, e2019WR026574. [CrossRef]
103. Jemberie, M. Evaluation of land use land cover change on stream flow: A case study of dedissa Sub Basin. *Int. J. Innov. Eng. Res. Technol.* **2016**, *3*, 44–60.